Mosab Nasser\*, Maersk Oil Houston Inc., Gary Mavko and Jack Dvorkin, Rock Physics Group, Stanford University, Gary Ostroff Maersk Oil Houston Inc.

### **Summary**

Well logs from deepwater Angola are texturally interpreted using a combination of petrophysical and rock physics models. The Thomas-Stieber model predicts the porosity resulting from various modes of sand-shale mixing. The Yin-Marion-Dvorkin-Gutierrez model predicts the associated P-wave velocities. Together, they offer a higher degree of constraint of formation properties.

#### Introduction

Thomas and Stieber (1975, 1977) presented a model (TS) describing the porosity-shale volume (Vsh) relations in clastic sediments. The TS model considers a range of lithologies, all of which can be constructed by mixing clean sand (quartz grains) and shale end-members. The TS model deals only with *volumetrics*. Yin (1992) and Marion (1990) developed an analogous clastics model (YM) for the *elastic* properties of clastic sediments composed of the same sand and shale end members.

This paper shows that coupling the TS and YM models can help to better constrain the interpretation of well logs by simultaneously modeling porosity, vshale, and P-wave velocity. Results are presented from a deepwater environment, offshore Angola.

### Geologic setting and lithologies

In this study we have used well log data from offshore Angola. The focus of this study is on an area of about 700 sqkm in which two wells were drilled. These two wells are used as the basis for our conclusions, which could potentially be extrapolated to other wells in the area. Target reservoirs in this area are found at different depths and deposited in middle to lower slope settings, following the trend of many of the deep water reservoirs in this area, which vary in style and consist of strongly to moderately confined channel systems that are typically sinuous, leveed and local ponded to distributive systems.

The base of most of the channel systems in this basin is dominated by a high impedance reflection on seismic interpreted to consist of gravelly turbidites. In contrast, mid to upper parts of the channel system are low impedance dominated, and are interpreted to consist of sandy turbidites and interbedded shales. Depending on the depth of the sand, Class I, II and IIP AVO can be interpreted using angle seismic substacks. The seismic data

in this area is considered of a reasonable quality to be used for AVO analysis.

#### Integrated petrophysical-rock physics models

Thomas and Stieber (1975, 1977) developed a model for the porosity of thinly bedded sands and shales, under the assumption that all rocks in the interval, including dirty sands, can be constructed by mixing clean sand and shale. Figure 1 illustrates some of the lithologies that they considered. Shale (row 1), with porosity  $\phi_{shale}$  is one endmember, and clean sand (row 2), with porosity  $\phi_{clean-sand}$ is the second end-member. Lithology 3 is dirty sand, in which some of shale lies within the sand pore space (also referred to as 'dispersed shale'). As long as the volume of shale  $V_{sh}$  is less than  $\phi_{clean-sand}$ , the model assumes that the sand grain packing is undisturbed. Lithology 4 is an extreme of lithology 3 in which  $V_{sh} = \phi_{clean-sand}$ Lithology 5 has shale fractions  $1 \le V_{\mathit{sh}} \le \phi_{\mathit{clean-sand}}$ , so that sand grains are floating in the shale. Lithology 6 is a special case in which sand grains in lithologies 2, 3, or 4 are replaced by structural shale clasts. Additional lithologies are modeled as thinly interbedded laminations of shale (1) and any of the sands (1-3). A recent summary of the model can be found, for example, in Mavko et al. (2009).

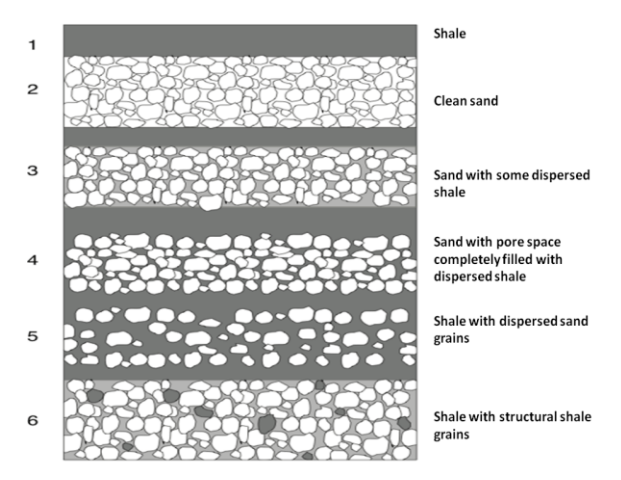


Figure 1: Various sand-shale mixtures within the Thomas-Stieber model.

Figure 2 shows the resulting total porosity-shale relations predicted by the TS model. Point A is the clean sand; C is

the shale. Line A-B shows the trend of increased dispersed shale (lithologies 2-4 in Figure 1). Line B-C shows the trend of silt/sand grains replaced with shale matrix (lithology 5). Constant values of sand lamination porosity are defined by lines radiating from C; for example, C-A is laminated shale and clean sand; C-F if laminated shale and dirty sand. Lines parallel to A-B contour net-to-gross (NG), so that for example, a rock plotting at point E would be interpreted as 60% sand laminated with 40% shale, and the sand has a volume fraction of dispersed shale equal to  $0.4 \, \phi_{clean-sand}$ .

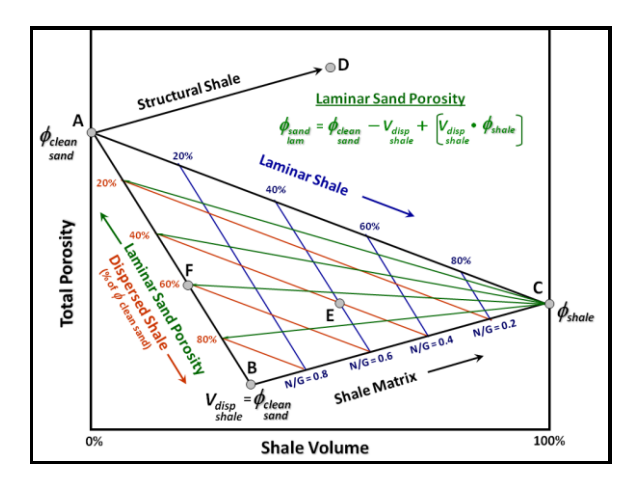


Figure 2: Total porosity vs. shale volume, as predicted by the Thomas-Stieber model.

Based on lab measurements on sand-kaolinite mixtures, Yin (1992) and Marion (1990) developed an analogous model (YM) for relations among seismic velocity, porosity, and shale fraction (Marion and Nur, 1991; Marion et al., 1992; Nur and Marion, 1991). The YM model is illustrated in Figure 3. End members are clean sand (A) and shale (C). Dispersed shale in sand increases along A-B. Point B corresponds to the original sand pore space completely filled with dispersed shale. From B to C sand/silt grains are being replaced with shale matrix. The dashed line A-C is the approximate trend for thin laminations of the sand and shale end members.

Marion (1990) and Dvorkin and Gutierrez (2002) showed how to model (MDG) velocity vs. porosity by combining the TS model for porosity-Vshale and the YM model for Vp-Vsh (Figure 4). Here, once again, A is the clean sand end-member, C is the shale end-member, dispersed shale increases along A-B, and sand/silt grain are increasingly replaced with shale matrix from B to C. Laminations of sand and shale fall along A-C. Figure 4 also shows the "suspension line," which is computed using the Reuss average of the mineral and pore fluid moduli and is a lower

bound. The "clean sand line" is computed using a modified Voigt average trending between the clean sand critical porosity

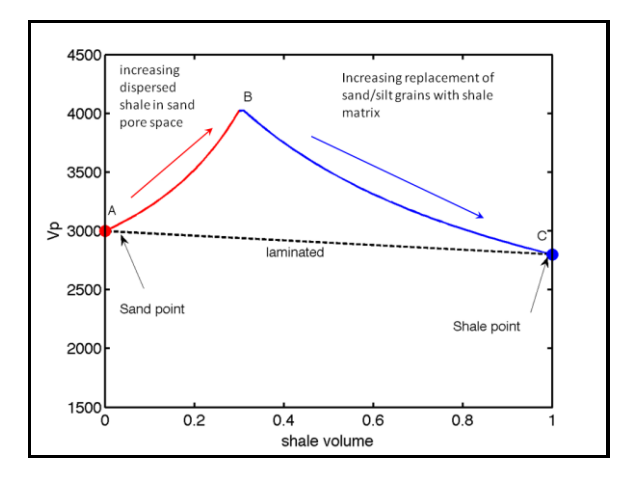


Figure 3: Velocity vs. shale volume, as predicted by the Yin Marion model

 $(\phi_c = 0.4)$  in this case) and pure mineral at  $\phi = 0$  (Dvorkin et al, 1991; Dvorkin and Nur, 1996). (The modified Voigt is slightly steepened near critical porosity to reflect the rapid stiffening when new sediments are initially compacted and/or cemented.) The curves AB and BC in Figure 4 are modeled using modified lower Hashin-Shtrikman (HS<sup>-</sup>) or Reuss curves (Dvorkin and Nur, 1996). In this application, the HS<sup>-</sup> and Reuss curves serve as *trend lines*, not bounds. They serve as *soft interpolators*, between the properties of the end-members (sand or shale) and the point B, where the shale-filled sand has its highest velocity.

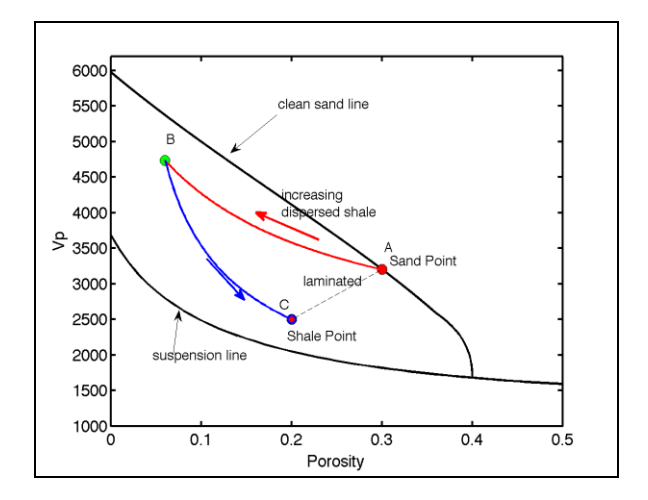


Figure 4: Velocity vs. porosity, as predicted by the Marion-Dvorkin-Gutierrez model.

## Application to field data

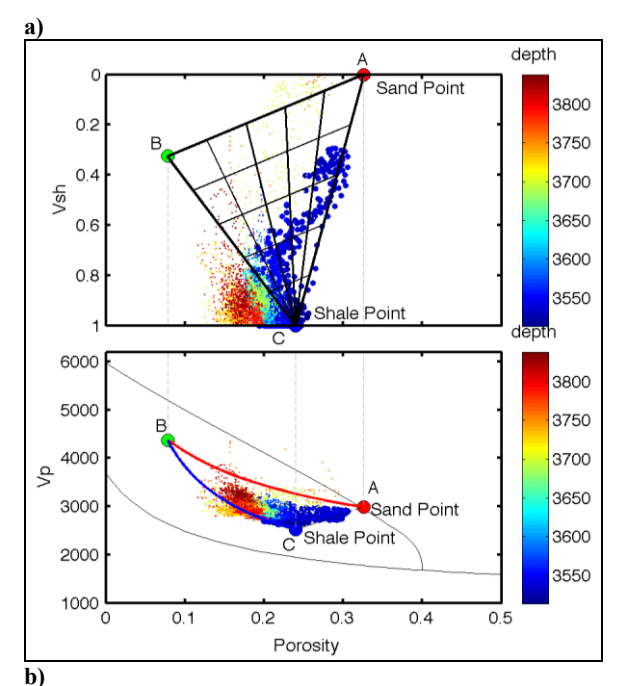
Figure 5 shows the hybrid model that can be obtained through coupling the TS model (Figure 2), the YM model (Figure 3), and the MDG model (Figure 4). The only independent variables are the end-member sand and shale properties, ( $\phi_{clean-sand}$ ·  $V_{P-clean-sand}$ ) and ( $\phi_{shale}$ ·  $V_{shale}$ ). Other porosity-velocity-shale lithologies are computed from the models in terms of the end-members. The lowermost plots in Figures 5a and 5b are the same as Figure 4. The uppermost plots in Figures 5a and 5b are the same as Figure 2, but rotated, so that all horizontal axes in Figure 5 represent total porosity.

The data in Figure 5 are from the West Africa well, colored by depth. Substantial depth variations, associated with compaction, can be seen in the sand and shale porosities. The model curves in Figure 5a are fit to the shale and sand end-members in shallow interval ~3550m, and the model curves in Figure 5b are fit to the shale and sand end-members in deeper interval ~3800m. The sand point A is constrained to lie along the clean sand line in the Vp-Porosity plots, while both point A and point C are constrained to best contain the data within the pair of three-sided figures. A consistent model fit also results in a rock plotting in both the Vsh-porosity and Vp-porosity planes lying at the same relative positions within the ternary figures; e.g., a laminated mix of 60% sand and 40% shale should plot at the same locations in each plot.

Figure 6 shows data from the shallow interval (~3550m) with the same model fit as in Figure 5a, but now the data are colored by lithofacies (6a) and Sw (6b). We note that the pay zone (low Sw) lies in thinly bedded packages of clean sand and shale (net-to-gross  $\sim 0.5$ -0.7), which have been interpreted as a zone of high-concentration turbidites. Lithofacies symbols in Figure 6 are as (silty-shaley MR=mudrocks non-reservoir facies); LCT+VLCT=low concentration and very low concentration turbidites; INJ=injectites; HCT=high concentration TRAC=traction turbidites; (gravelly, pebbly, conglomerate).

#### Conclusions

Well logs from offshore Angola are texturally interpreted using a combination of petrophysical and rock physics models. The Thomas-Stieber model predicts the porosity resulting from various modes of sand-shale mixing. The Yin-Marion-Dvorkin-Gutierrez model predicts the associated P-wave velocities. Together, they offer a higher degree of constraint of formation properties.



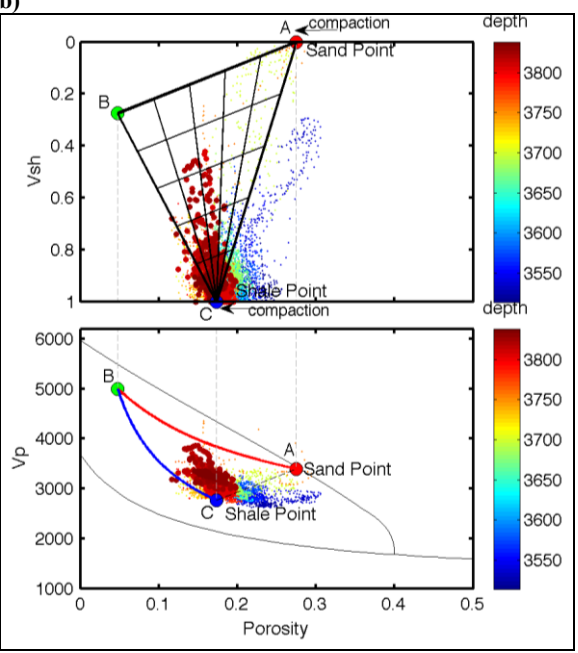


Figure 5: Hybrid T-S-Y-M model. a) sand and shale points fit to  $\sim$ 3550m; b) compaction of sand and shale points to  $\sim$ 3800m.

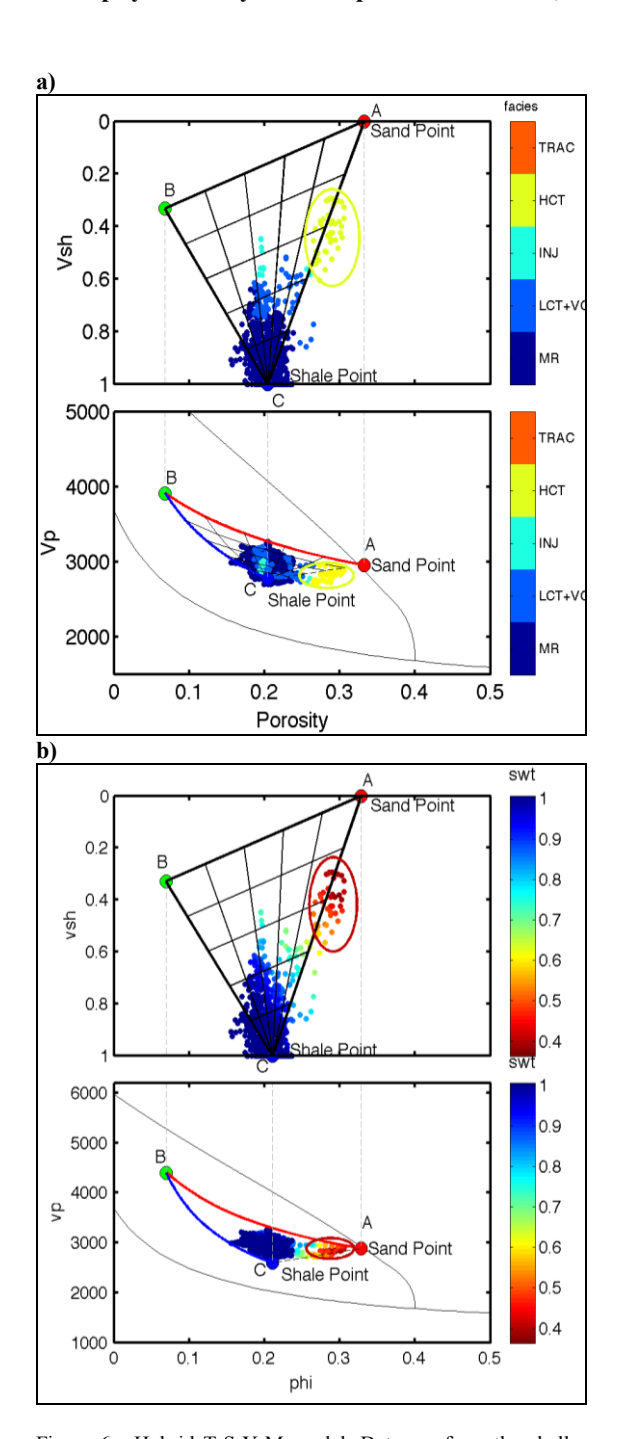


Figure 6: Hybrid T-S-Y-M model. Data are from the shallower interval and model sand and shale points fit to ~3550m. a) Data colored by petrophysical facies; b) data colored by Swt. Pay zone in high-concentration turbiditic interval are highlighted by ellipses. Facies are defined in the text.

The combined models are most applicable in poorly consolidated sediments, where porosity and elastic moduli are dominated by the dispersed and laminar mixing modes of sand and shale. An advantage of the models is that the entire set of represented lithologies follows from only a single pair of clean sand and shale end-members. If sand and shale have measureable compaction within the intervals of interest, then the corresponding models grids will deform with the end-member properties. Model accuracy degrades when deviations from the idealized mixing occur. For example, disturbances to the sand pack at small shale fractions can lead to larger total porosity than predicted by the model. Large compositional variations to shale properties within small depth intervals will add uncertainty. The presence of cement also complicates interpretation - cement can reduce pore volume without an increase in shale volume; cement will also tend to increase elastic moduli much more than the same volume of shale.

In situations where the model is appropriate, the combined use of porosity (density), shale volume (e.g., gamma ray), and Vp (sonic) data adds more confidence to interpreting the sediment pore texture. With calibration, the combination of sonic and porosity data yields information about reservoir quality.

### Acknowledgements:

We thank Maersk Oil and its partners Sonagol, Devon and Odebrecht oil & gas for permission to present this material. We also thank Maersk Oil's Angola team for their support throughout this work.

#### **EDITED REFERENCES**

Note: This reference list is a copy-edited version of the reference list submitted by the author. Reference lists for the 2011 SEG Technical Program Expanded Abstracts have been copy edited so that references provided with the online metadata for each paper will achieve a high degree of linking to cited sources that appear on the Web.

#### REFERENCES

- Dvorkin, J., and Gutierrez, M., 2002, Grain-sorting, porosity, and elasticity: Petrophysics, 43.
- Dvorkin, J., G. Mavko, and A. Nur, 1991, The effect of cementation on the elastic properties of granular material: Mechanics of Materials, **12**, no. 3–4, 207–217, <u>doi:10.1016/0167-6636(91)90018-U</u>.
- Dvorkin, J., and A. Nur, 1996, Elasticity of high-porosity sandstones: Theory for two North Sea datasets: Geophysics, **61**, 1363–1370, doi:10.1190/1.1444059.
- Mavko, G., T. Mukerji, and J. Dvorkin, 2009, The rock physics handbook: Cambridge University Press, 2nd ed.
- Marion, D., 1990, Acoustical, mechanical, and transport properties of sediments and granular materials: Ph.D. thesis, Stanford University.
- Marion, D., and A. Nur, 1991, Pore-filling material and its effect on velocity in rocks: Geophysics, **56**, 225–230, doi:10.1190/1.1443034.
- Marion, D., A. Nur, H. Yin, and D. Han, 1992, Compressional velocity and porosity in sand-clay mixtures: Geophysics, **57**, 554–563, doi:10.1190/1.1443269.
- Nur, A., D. Marion, and H. Yin, 1991, Wave velocities in sediments, *in* J. M. Hovem, ed., Shear waves in marine sediments: Kluwer Academic Publishers, 131–140.
- Thomas, E. C., and S. J. Stieber, 1975, The distribution of shale in sandstones and its effect upon porosity: Transactions of the 16th Annual Logging Symposium of the SPWLA, Paper T.
- ———, 1977, Log-derived shale distributions in sandstone and its effect upon porosity, water saturation, and permeability: Transactions of the 6th Formation Evaluation Symposium of the Canadian Well Logging Society.
- Yin, H., 1992, Acoustic velocity and attenuation of rocks: Isotropy, intrinsic anisotropy, and stress-induced anisotropy: PhD thesis, Stanford University.